PHYSICAL REVIEW B **87**, 125137 (2013)

Thin metamaterial Luneburg lens for surface waves

J. A. Dockrey, M. J. Lockyear, S. J. Berry, S. A. R. Horsley, J. R. Sambles, and A. P. Hibbins
Electromagnetic and Acoustic Materials Group, Department of Physics and Astronomy, University of Exeter, Stocker Road, Exeter EX4 4QL, United Kingdom
(Received 30 November 2012; published 22 March 2013)

By suitably patterning a metasurface, the phase velocity of surface waves may be manipulated. Here, a low-loss, thin (1/14th of the free-space wavelength), omnidirectional Luneburg lens, based upon a Sievenpiper "mushroom" array [Sievenpiper *et al.*, IEEE Trans. Microwave Theory Tech. **47**, 2059 (1999)], is fabricated and characterized at microwave frequencies. Surface waves excited using a near-field point source on the perimeter of the lens, exit the opposite side of the lens as planar wave fronts. The electric field of the surface wave is mapped out experimentally and compared to numerical simulations.

DOI: 10.1103/PhysRevB.87.125137 PACS number(s): 41.20.Jb, 42.25.Bs, 73.20.At, 78.67.Pt

The study of electromagnetic (EM) surface waves confined at the interface between two dissimilar media has generated much theoretical and experimental interest since the late 19th century.[1–4] Waves that propagate at the planar interface between a metal and a dielectric are transverse magnetic (TM) polarized, and at visible wavelengths, are characterized by exponentially decaying fields into both media. These "surface-plasmon polaritons," which have a dispersion defined primarily by the metals negative real, frequency dependent, dielectric constant, have generated a plethora of research.[5–7] At microwave frequencies metals are good conductors and possess a large and imaginary dielectric constant. The surface wave fields extend many wavelengths into the dielectric half space, while almost completely excluded from the metal. In this regime, these loosely bound surface modes are often simply described as surface currents. However, Pendry *et al.*[8] showed theoretically, and experiment has since confirmed[9] that subwavelength surface structure (i.e. a metasurface[10]) can bind the mode to the interface, leading to surface-plasmon-like behavior, even on perfect conductors. These metasurfaces have found applications such as antenna design at microwave frequencies.[10,11] One such example of a structure that supports TM surface waves is the Sievenpiper "mushroom" array;[12] a very thin metasurface that provides the necessary boundary condition to support a TM surface wave.[13] The lowest order resonance of this surface acts as a limit frequency to the TM surface wave, in the same way that the waveguide cutoff of Pendry's original hole array[8] provided a dispersion of the surface-plasmon form.[14] By engineering the dimensions of the mushroom[15] elements across the array, the phase velocity of the surface mode can be controlled (termed "metasurfing"[10]), and the propagation of the surface mode manipulated. Note that this phase velocity, which a measure of the mode index, i.e., $n_{SW} = c/v_{\text{phase}}$, is not a property of the bulk material but a measure of how far the surface wave dispersion deviates from the light line. For the Sievenpiper mushroom surface considered in the present work, we vary the side length of the patches, a (Fig. 1), across the surface to create a thin, low-loss, Luneburg lens for TM surface waves.

The free-space Luneburg lens[16–18] is a well-known device that focuses radiation emitted from a point source located on its perimeter to a plane wave emanating from the diametrically opposite side of the lens (or vice versa), using a refractive index profile that decreases radially from its center.[19] Such devices have been experimentally realized as a series of concentric rings,[20,21] where the refractive index is varied in steps rather than as a smooth function of radius. Additionally, devices have been designed by simplifying the problem into two dimensions, by utilizing a two-dimensional (2D) metamaterial that supports bulk electromagnetic modes.[22] Note that although these freestanding metasurface devices utilize 2D optics, they are not designed for surface waves. Such devices have found applications ranging from wireless communication systems[23] to Doppler weather radar.[24]

A Luneburg lens for TM surface waves was first proposed in 1960,[25] where the mode index profile was realized both by tailoring the thickness of a polystyrene overlayer, and by arranging a series of cylindrical posts of varying height on a ground plane. In 2001, Park *et al.*[26,27] designed and fabricated a Luneburg lens for TM surface waves comprised of a square array of square posts of varying height on a ground plane. A surface wave Luneburg lens has also been devised and characterized for transverse electric (TE) surface waves,[14] in which three concentric rings of circular holes of different sizes are etched in a square lattice on the top plate of a dielectric filled parallel metal plate, providing the mode index profile.[28] However, in all of the experimental studies highlighted, the device has been characterized by measuring the far field radiation pattern. An optical study[29] and recent theoretical studies[11,30] have started to remedy this, although a detailed comparison between the experimentally measured and simulated instantaneous surface wave field profile is absent. In this paper, we present a direct and detailed comparison between the experimentally measured instantaneous electric field profile of surface waves propagating along the device with the predictions from numerical simulations. The mushroom elements that constitute the metasurface in this study enable the fabricated device to be thinner than the aforementioned devices, while it is important to note that the metasurface was not optimized for device thickness during the design process.

The mushroom metasurface [see Fig. 1(b), inset] provides a route to construct a sample which is very thin (∼1.6 mm, although it could be much thinner using higher index dielectric layers) compared to an operating wavelength of 23.1 mm. It is manufactured using standard printed circuit board (PCB) technology and comprises an array of square elements (of

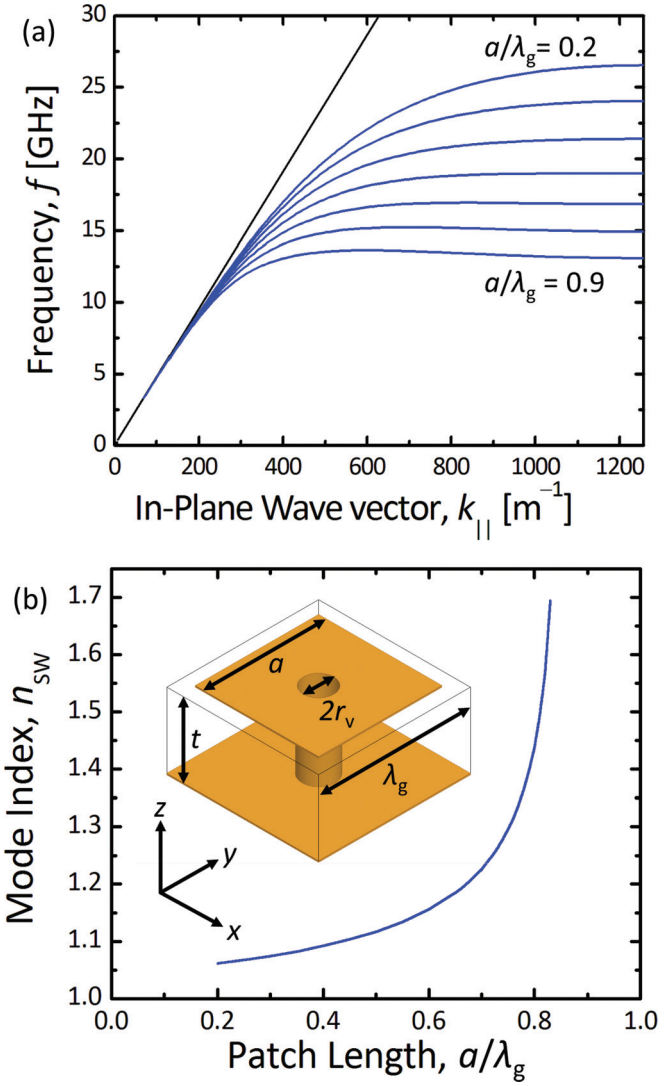

FIG. 1. (Color online) (a) Numerical predictions (Ref. 31) of the dispersion relation of a surface wave on an array of identical mushrooms, where each line corresponds to a different patch length, a. (b) Surface wave mode index n_{SW} as a function of patch length at 13.0 GHz. Inset: Schematic of the mushroom unit cell.

varying size) arranged in a square lattice of pitch $\lambda_g = 2.5$ mm, using 12-μm-thick copper cladding on either side of a low-loss 1.6-mm-thick (t) dielectric [Nelco NY-9220 ($\varepsilon_r = 2.22 + 0.002i$)] layer. Cylindrical copper vias of radius $r_v = 175$ μm are located at the center of each patch. The patch side length a is tailored for the required mode index $n_{SW}(r)$ in accordance with that necessary for a Luneburg lens,[19]

$$n_{SW}(r) = \begin{cases} N\sqrt{2 - \left(\frac{r}{R}\right)^2}, & r \leqslant R \\ N, & r > R \end{cases} \quad (1)$$

Here, r is the distance away from the center of the lens, R is the radius of the Luneburg lens, and N represents a scale factor ($N = 1.06$ for this device, which defines the mode index of the surface wave on the metasurface away from the lens). However, only within the approximation of geometrical optics can one simply multiply an index profile by a constant and obtain the same functionality, given that the optical size of the device will

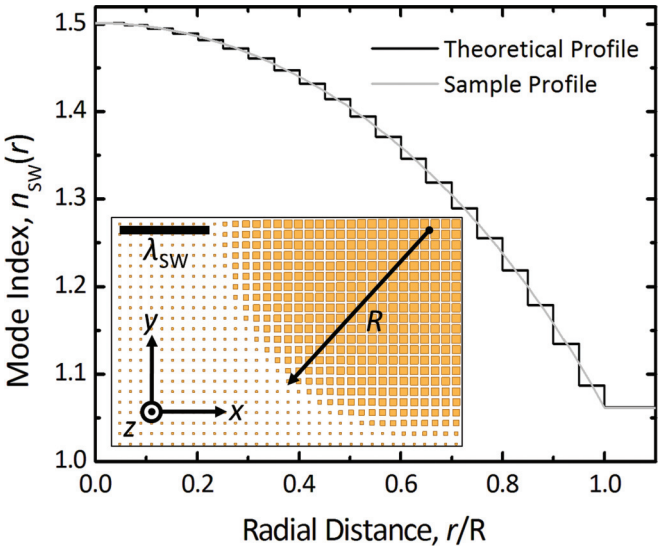

FIG. 2. (Color online) A comparison between the ideal Luneburg lens mode index profile and the stepped mode index profile of the fabricated device taken along a radial distance parallel to the lattice, where the discrete steps are a consequence of the finite pitch of individual mushroom elements. Inset: Schematic of a section of the thin Luneburg lens from above, demonstrating the change in mushroom patch length a, throughout the device. The scale bar provides a comparison of the size of the device to the wavelength of surface waves as they traverse the background medium λ_{SW}.

change depending on the value of the scale factor. In this study, the geometrical approximation is reasonably valid with the diameter of the lens being of the order of five wavelengths. The radial distance (r) from the center of the device to the center of each patch is taken as the distance used to calculate the required mode index of each unit cell, and given that each unit cell is significantly subwavelength ($\lambda_g \sim \lambda_0/9$), the resultant device will be omnidirectional.

A finite element method model[31] is used to simulate the response of an array of identical elements, allowing dispersion curves of the fundamental TM mode to be extracted for structures of a given patch size [Fig. 1(a)]. It is clear that as the patch size is increased, the asymptotic frequency of the surface wave dispersion is reduced. As the mode diverges from the light line the phase velocity of the propagating surface wave is reduced, resulting in a higher mode index. Here, the mode index is determined at 13.0 GHz as a function of patch size [Fig. 1(b)], which is then utilized to design the required surface structure by arranging mushroom unit cells of appropriate patch size in a periodic array (for a schematic of the device see Fig. 2, inset). This design technique allows the narrow-band device to be tuned to any operating frequency, with the primary restrictions being the thickness of available PCB and the upper limit in the periodicity of the elements to avoid strong spatial dispersion.[32]

To design the Luneburg lens, an important assumption is made: that it is possible to assign a macroscopic quantity of a surface wave on an array of identical elements (mode index) to a single microscopic element (unit cell), i.e., that a single mushroom with nonidentical nearest neighbors induces the same boundary condition as a mushroom in an array of

identical elements. From Eq. (1), it is possible to determine the required mode index for a unit cell given its radial distance from the center of the device (r) and from this mode index, the required patch size can be extrapolated from the data illustrated in Fig. 1(b). With the resonant nature of the structure leading to an exponential-like relationship between the side length of the patch (a) and mode index (n_{SW}), it is necessary to minimize the effect of fabrication tolerances on the performance of the device. The minimum patch side length (a) is chosen to be 500 μm, providing a background mode index of 1.06 (hence, $N = 1.06$) at the chosen operating frequency of 13.0 GHz.

In the experiment, surface wave excitation and detection is achieved through the use of a pair of near-field probes. They are each 2.1-mm-diameter coaxial cables, cut to ensure that the 0.5-mm-diameter inner wire was exposed to a length of 2.5 mm at one end. The experimental arrangement is such that both probes were oriented with the inner wire normal to, and at a height of ~1 mm above the surface. When detecting TM surface waves, this setup minimizes the detection of the electric field along the direction of propagation ($E_{||}$) while maximizing the detection of the electric field normal to the surface (E_z). The source and detector antennas are connected to a vector network analyzer (VNA) for measurements of electric field magnitude and phase difference $\Delta\phi$ (between the detected and an internally referenced signal within the VNA). One antenna is placed on the perimeter of the Luneburg lens to act as a near-field source for surface waves and the other antenna (detector) is moved in the xy plane by a motorized stage. Note that the approximation of geometrical optics is not completely valid here with the limited size of the structure relative to the wavelength expected to be detrimental to performance.[33,34]

It is important to note that the VNA and near-field probe measurement technique records time-averaged electric field magnitudes. In order to qualitatively examine the performance of the Luneburg lens, it is useful to also derive the instantaneous fields from the experimentally obtained phase information and time-averaged field data [see Fig. 3(a)]. The equivalent numerical simulation is shown in Fig. 3(b), where the instantaneous magnitude of E_z is shown in a plane 2.25 mm above the surface (for animations, see Supplemental Material[35]). This plane is chosen because it represents the plane halfway up the exposed length of the antenna used in the experiment. The color scales on both plots are normalized using reference values of the field magnitude in the top left and right regions of each plot; regions where radiation emitted from the point source does not traverse the Luneburg lens. One of the antennas is placed at the focus of the Luneburg lens on its perimeter ($x = 0$ mm, $y = 50$ mm), and the resulting field intensity across the sample demonstrates the characteristic behavior of a Luneburg lens,[19] with the wavelength of the surface wave reducing appropriately in the region of high mode index (near its center). Because the diameter of the device is 100 mm, a little over four times its operational wavelength (a limit imposed by the size of the available PCB board), the interference effects show deviations from the approximation of geometrical optics,[36] which are also demonstrated in the simulations.

A full numerical model of even this relatively small (compared to the operation wavelength) device is extremely computationally intensive since the tetrahedral mesh must adequately represent more than 1500 mushroom elements. Therefore, an impedance sheet approximation[31] is employed that replaces the surface structure with a simple boundary condition, dictated by the ratio of the electric to magnetic field tangential to the surface; the surface impedance Z_S. One can relate the spatially varying mode index [Eq. (1)] to an inhomogeneous Z_S as follows. The free space Maxwell

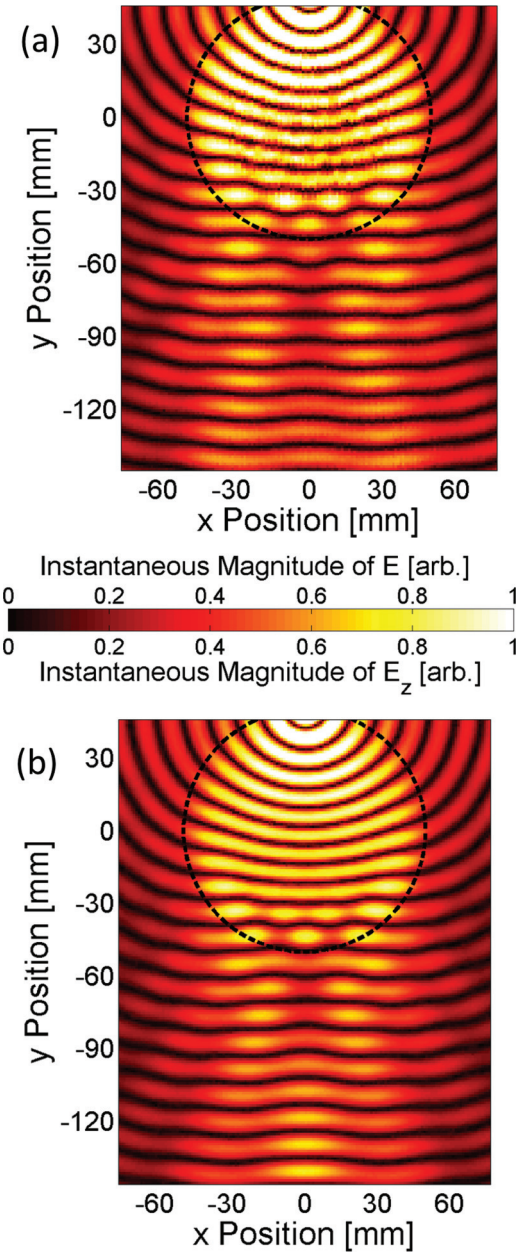

FIG. 3. (Color online) (a) Electric field magnitude data taken in a plane ~1 mm above the surface wave Luneburg lens sample, using a near-field antenna as a point source for surface waves at ($x = 0$ mm, $y = 50$ mm) at 13 GHz. (b) Simulation of the instantaneous magnitude of the E_z field above the same device at 13 GHz, using an impedance sheet approximation in the finite element method model. Both plots were normalized to the same color magnitude scale using the magnitude of the cylindrical wave fronts in the top corners of the two plots as a reference; regions where the surface waves do not traverse the Luneburg lens.

equations $\nabla \Lambda E = i\omega B$ and $\nabla \Lambda B = (i\omega/c^2)E$ are rewritten in terms of their tangential and normal components, e.g., $E = E_z\hat{z} + E_{||}$, etc. Combining the two Maxwell equations above, and setting the boundary conditions $B_z = 0$ and $\hat{z}\Lambda E_{||} = \mu_0^{-1} Z_S B_{||}$ (Ref. 37) at the surface ($z = 0$) then yields

$$\left[\nabla_{\parallel}^2 + \frac{\omega^2}{c^2}\left(1 - \frac{Z_S^2}{\eta^2}\right)\right] B_{\parallel} = -\frac{i\omega}{\mu_0 c^2} B_{\parallel} \left.\frac{\partial Z_S}{\partial z}\right|_{z=0}, \quad (2)$$

where we have applied the condition $\nabla_{\parallel} \cdot B_{\parallel} = 0$ in the final step, and with $\eta = \sqrt{\mu_0/\varepsilon_0}$ is the impedance of free space. The speed of light in vacuum and the angular frequency of the wave are represented by c and ω, respectively. The quantity $\partial Z_S/\partial z$ is unknown and determines the extent to which the wave is bound to the surface. For a surface wave bound to a homogeneous medium, $\partial Z_S/\partial z = 0$, due to the z dependence of both the E and B fields being the same. It is assumed that if the impedance varies slowly enough over the surface there will be limited scattering into free space and the right-hand side of Eq. (2) can be approximately set to zero. It is then clear that the surface waves obey the two-dimensional Helmholtz equation with a mode index $n_{SW}(r,\omega)$ of

$$n_{SW}(r,\omega) = \sqrt{1 - \frac{Z_S(r,\omega)^2}{\eta^2}}, \quad (3)$$

where r is the position vector in the plane of the surface. In the homogeneous case, this reduces to the expression given in Ref. 38. The simple mode index profile of the Luneburg lens [Eq. (1)] leads to a purely imaginary (reactive) surface impedance. Since impedance sheet models demand a complex surface impedance, $Z_S = R_S + i\chi_S$, the surface resistance is assigned a value of $10^{-6}\ \Omega$ (hence $Z_S \sim i\chi_S$); negligible losses are therefore assumed in the simulations.

In this study, we present a technique for tailoring the mode index of surface waves by modifying the patch length of constituent mushroom elements within a metasurface. As a demonstration of this methodology, we design, fabricate using standard PCB technology, and fully characterize a very thin, low-loss, omnidirectional Luneburg lens for TM surface waves operating at a frequency of 13.0 GHz. The metasurface comprises a square array of square mushroom elements and has an overall thickness of 1.6 mm compared to a free-space operational wavelength of 23.1 mm. A variation in the patch size, depending on its radial location within the device, achieves the required mode index profile for the Luneburg lens. Our surface wave experiments allow for the direct measurement of the electric fields within the lens, which is otherwise problematic in 2D or 3D transformation optics devices. The predictions from a numerical model, which utilizes an impedance sheet approximation, show excellent agreement with our experimental field data.

The authors wish to acknowledge financial support from the EPSRC through the University of Exeter's Doctoral Training Account, and also for support through the QUEST programme grant (EP/I034548/1) "The Quest for Ultimate Electromagnetics using Spatial Transformations (QUEST)." S.A.R.H. also acknowledges the EPSRC for its financial support. We also wish to thank BAE Systems for supporting S.J.B. through an EPSRC industrial case studentship.

[1] A. Sommerfeld, Ann. Phys. **67**, 233 (1899).
[2] K. Uller, Ph.D. thesis, University Rostock, 1903.
[3] J. Zenneck, Ann. Phys. **23**, 846 (1907).
[4] A. Sommerfeld, Ann. Phys. **28**, 665 (1909).
[5] R. H. Ritchie, Phys. Rev. **106**, 874 (1957).
[6] W. L. Barnes, A. Dereux, and T. W. Ebbesen, Nature (London) **424**, 824 (2003).
[7] S. C. Kitson, W. L. Barnes, and J. R. Sambles, Phys. Rev. Lett. **77**, 2670 (1996).
[8] J. P. Pendry, L. Martin-Moreno, and F. J. Garcia-Vidal, Science **305**, 847 (2004).
[9] A. P. Hibbins, B. R. Evans, and J. R. Sambles, Science **308**, 670 (2005).
[10] S. Maci, G. Minatti, M. Casaletti, and M. Bosiljevac, IEEE Antennas Wireless Propag. Lett. **10**, 1499 (2011).
[11] M. Bosiljevac, M. Casaletti, F. Caminita, Z. Sipus, and S. Maci, IEEE Trans. Antennas Propag. **60**, 4065 (2012).
[12] D. Sievenpiper, L. Zhang, J. B. Broas, N. Alexopolous, and E. Yablonovitch, IEEE Trans. Microwave Theory Tech. **47**, 2059 (1999).
[13] M. J. Lockyear, A. P. Hibbins, and J. R. Sambles, Phys. Rev. Lett. **102**, 073901 (2009).
[14] A. P. Hibbins, M. J. Lockyear, and J. R. Sambles, Phys. Rev. B **84**, 115130 (2011).
[15] N. I. Zheludev, Science **328**, 582 (2010).
[16] S. P. Morgan, J. Appl. Phys. **29**, 1358 (1958).
[17] G. D. M. Peeler and D. H. Archer, IRE Trans. Antennas Propag. **1**, 12 (1953).
[18] H. Ma, X. Chen, X. Yang, H. Xu, Q. Cheng, and T. Cue, Chin. Sci. Bull. **55**, 2066 (2010).
[19] R. K. Luneburg, *The Mathematical Theory of Optics* (University of California Press, Berkeley, 1964).
[20] L. C. Gunderson and G. T. Holmes, Appl. Opt. **5**, 801 (1967).
[21] Y. L. Loo, Y. Yang, Y. G. Ma, and K. C. Ong, J. Opt. Soc. Am. A **29**, 426 (2012).
[22] A. Cheng, H. F. Ma, and T. J. Cui, Appl. Phys. Lett. **95**, 181901 (2009).
[23] J. George, P. F. M. Smulders, and M. H. A. J. Herben, Electron. Lett. **37**, 73 (2001).
[24] R. M. Thompson, Proceedings of the 19th Digital Avionics Systems Conference, Philadelphia, 2000 (unpublished).
[25] C. H. Walter, IRE Trans. Antennas Propag. **8**, 508 (1960).
[26] Y. J. Park and W. Wiesbeck, IEEE Antennas Wireless Propag. Lett. **1**, 128 (2002).
[27] Y. J. Park, A. Herschlein, and W. Wiesbeck, IEEE Trans. Microwave Theory Tech. **49**, 1854 (2001).
[28] L. Xue and V. F. Fusco, Microwave Opt. Technol. Lett. **50**, 378 (2007).
[29] T. Zentgraf, Y. Liu, M. H. Mikkelsen, J. Valentine, and X. Zhang, Nat. Nanotechnol. **6**, 151 (2011).

[30]M. Casaletti, F. Caminita, and S. Maci, Proceedings of the Fourth European Conference on Antennas and Propagation (EuCAP), Barcelona, Spain, 2010 (unpublished).
[31]Ansoft Corporation, Ansoft HFSS, Pittsburgh, PA, www.ansoft.com/products/hf/hfss/.
[32]A. I. Cabuz, D. Felbacq, and D. Cassane, Phys. Rev. A **77**, 013807 (2008).
[33]P. Rozenfeld, IEEE Trans. Antennas Propag. **24**, 365 (1976).
[34]K. Mori, S. Yamaguchi, and T. Hosono, Electron. Commun. Jpn., Part 2: Electron. **70**, 73 (1987).
[35]See Supplemental Material at http://link.aps.org/supplemental/10.1103/PhysRevB.87.125137 for animations in phase of both the simulated and experimentally obtained field plots of the Luneburg lens.
[36]U. Leonhardt and T. Philbin, *Geometry and Light: The Science of Invisibility* (Dover, New York, 2010).
[37]P. M. Morse and H. Feshbach, *Methods of Theoretical Physics: Part 1* (McGraw-Hill, New York, 1953).
[38]S. Tretyakov, *Analytical Modeling in Applied Electromagnetics* (Artech House, Norwood, MA, 2003).